Journal of Power Sources 414 (2019) 96–102

Contents lists available at ScienceDirect

Journal of Power Sources

journal homepage: www.elsevier.com/locate/jpowsour

All carbon based high energy lithium-ion capacitors from biomass: The role of crystallinity

Palanichamy Sennu[a,b], Nagasubramanian Arun[c], Srinivasan Madhavi[b], Vanchiappan Aravindan[d,*], Yun-Sung Lee[a,**]

[a] Faculty of Applied Chemical Engineering, Chonnam National University, Gwang-ju, 500-757, Republic of Korea
[b] School of Materials Science and Engineering, Nanyang Technological University, 639798, Singapore
[c] TUM-CREATE LTD, #10-03, CREATE Tower, 1 Create Way, 138602, Singapore
[d] Department of Chemistry, Indian Institute of Science Education and Research (IISER), Tirupati, 517507, India

HIGHLIGHTS

- High-performance Li-ion capacitor (LIC) is assembled using bio-mass derived carbons.
- Semi-crystalline carbon is used as Battery type electrode than usual ordered phase.
- This LIC is capable of delivering the maximum energy density of ~216 Wh kg^{-1}.

GRAPHICAL ABSTRACT

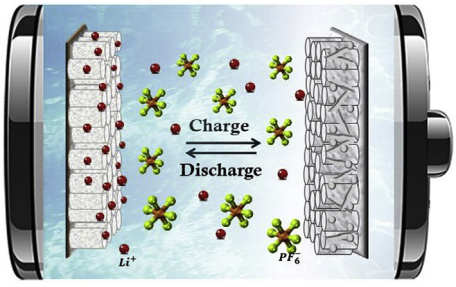

ARTICLE INFO

Keywords:
Lithium-ion capacitor
Few-layer graphene
Bio-waste
Energy density

ABSTRACT

We report all carbon-based high energy Li-ion capacitor from environmentally threatening bio-source, *prosopis juliflora*. The pyrolyzed carbon exhibits a few layers of graphene-like structure and tubular morphology with multiple inherent heteroatoms like N, S, and Ca. Presence of such heteroatoms are certainly beneficial to the betterment of electrical conductivity, and pore generation which eventually results in an enhancement in capacity/capacitance of carbonaceous materials. The electrochemical pre-lithiation strategy is used to mitigate the irreversibility observed, and eventually employed as a negative electrode in a hybrid configuration. This LIC delivered a high energy density of ~216 and 185 Wh kg^{-1} at ambient (25 °C) and elevated temperature (55 °C) conditions, respectively. Further, ~94% initial capacity is retained after 5000 cycles with minimum fading of 0.0013% per cycle at ambient temperature. This results clearly demonstrate that the surface functionality and heteroatom doping with tubular structure synergistically facilitates the Li^+ and electron transport properties to realize higher energy density for this fascinating all carbon-based Li-ion capacitor.

1. Introduction

Environmentally friendly, fast and high energy storage features with lightly weighted devices are of particular interest, and under development for electric vehicles, smart grid and many other industrial prospects. A supercapacitor is considered a promising charge storage device, but it falls apart in terms of the long-term and sufficient energy deliverability [1]. In this respect, the Li-ion battery is recognized as an

* Corresponding author.
** Corresponding author.
E-mail addresses: aravind_van@yahoo.com (V. Aravindan), leeys@chonnam.ac.kr (Y.-S. Lee).

https://doi.org/10.1016/j.jpowsour.2018.12.089
Received 10 October 2018; Received in revised form 29 December 2018; Accepted 31 December 2018
Available online 04 January 2019
0378-7753/

energy efficient system for portable devices, but their flaw is unable to attain a satisfactory power efficiency, cycling life, and cost-effectiveness. Amatucci et al. [2,3] first introduced the concept of a hybrid energy storage system which is anticipated by bridging the gap between battery and supercapacitor called Li-ion capacitor (LIC) [4]. So far, several intercalation, conversion, and alloy materials with high specific capacity were proposed as a negative electrode for LIC [5–8].

In 1983, Yazami et al. [9,10] successfully demonstrated the reversible intercalation of Li-ions into the graphite electrode. Till date, graphite remains popular insertion anode for Li-ion battery perspective, besides a variety of carbon allotropes are explored as promising insertion hosts [11]. Amongst, amorphous carbon with some crystalline strands *i.e.* few-layer graphene is one of the promising battery electrodes for LIC perspective owing to the wider interlayer spacing (ca 0.47 nm), high theoretical capacity and low risk of lithium plating at a lower working potential (*vs.* Li). Presence of such amorphous domain certainly facilitates both electron and Li-ion transport, besides participating in electrochemical reaction *via* double layer formation along with Li-ion insertion in crystalline strands [12].

Recently, preparation of carbonaceous materials from inexpensive and renewable bio-sources gained special attention and increasing interest due to the environmental concerns, recycling, cost-effectiveness and beneficial properties like the presence of inherent hetero-atoms (N, S, P and Ca), surface functionalization etc., [13–15]. Further, it is well established that those features effectively improve the electrochemical activity of the carbonaceous electrodes regardless of either symmetric or asymmetric assemblies [16–19]. Till date, numerous bio-mass precursors have been explored towards supercapacitor point of view, but most of them are used in electric double layer capacitor with symmetric fashion or asymmetric assembly with metal oxide/sulfide in aqueous media [20–23]. For the utilization of such bio-mass derived carbonaceous materials in a hybrid configuration, specifically, all carbon-based LIC assembly is very limited. Since, in LIC assembly only one electrode undergo Faradaic reaction, whereas counter electrode should involve in the double layer formation *i.e.* non-Faradaic storage. Although there is a possibility to use metal oxide (eg. $Li_4Ti_5O_{12}$, TiO_2 etc.) as battery type insertion component instead of intercalation type carbonaceous materials like graphite and hard carbon, it is very difficult to realize the high energy density *viz.* achieving even 100 Wh kg^{-1} is not possible [5,6]. Therefore, amorphous carbon with crystalline strands *i.e.* few-layer graphene is one of the finest approaches to realize the high energy density without compromising power capability.

Among the diverse plant species, prosopis juliflora tree is widely available, and environmental threatening invasive weed, in which the timber is predominantly used as fuel, and making crafts and furniture. This species is known for its deep penetrating roots, it can go up to 50 feet depth to suck the available groundwater and eventually produce drought situation in and around. Hence, uprooting the species from the soil is mandatory for the human kind and environmental aspects [24,25]. In this paper, we report the possible utilization of such prosopis juliflora derived carbons (PJC) as both negative (intercalation type *i.e.* amorphous carbon with few-layer graphene, PJC) and positive (activated carbon, PJAC) electrodes to construct all carbon-based LIC assembly. Accordingly, the synthesis conditions are fine-tuned and efficiently utilized [26]. The preliminary Li-storage capability of PJC and PJAC were conducted in a half-cell (*vs.* Li metal), which is essential to balance the mass loading between the electrodes during the fabrication of LIC. In addition, the PJC was electrochemically pre-lithiated, and its electrochemical activity with PJAC was monitored in LIC assembly at both ambient (25 °C) and elevated temperature (55 °C) conditions and described in detail.

2. Experimental section

2.1. Preparation of carbonaceous materials

Naturally dried pieces of Prosopis juliflora wood harvested from the Indian soil and charred at 250 °C in an oven and then ground into fine powder by using mortar and pestle. Then, the black powder was heated at 900 (PJC-1) and 1000 °C (PJC-2) for 3 h under N_2 flow. Some portion of the powder was treated with 1:2 wt% of KOH and subsequently activated at 1000 °C for 3 h under N_2 flow (PJAC). After this activation process, the resultant product was repeatedly washed with hot water and ethanol, and subsequently vacuum dried at 80 °C for overnight. The dried black coloured powdered was subjected to further characterizations.

2.2. Physical characterization

The crystalline phase of a resultant material was studied by X-ray diffractometer (XRD, Rint 1000, Rigaku, Japan) using CuKα radiation. The N_2 adsorption/desorption isotherms were performed using a Micromeritics ASAP 2010 surface area analyzer. The surface morphological and internal structural aspects were analyzed with a scanning electron microscope (Hitachi-S4700) and high-resolution transmission electron microscope (TECNAI-F20 Philips). X-ray photoelectron spectroscopy (XPS) was also performed to ensure the presence of hetero-atoms and surface functionalities using Multilab 2000, UK with monochromater Al Kα radiation ($h\nu$ = 1486.6 eV).

2.3. Electrochemical characterizations

All the electrochemical measurements were performed in CR2032 coin-cell. The working electrodes were formulated with 74 wt % of active materials (PJC-1, PJC-2, and PJAC), 13 wt % of Ketzen black, and 13 wt % of teflonized acetylene black (13%, TAB-2) using ethanol. The slurry was pressed over a stainless-steel mesh (200 mm^2 area) and dried at 160 °C for 4 h under vacuum. The half-cell and LIC assembly were constructed with two electrode configuration separated by porous polypropylene (Celgard 3401, USA) film and gelled with 1 M $LiPF_6$ solution with a mixture of 1:1 vol/vol ethylene carbonate/di-methyl carbonate (Soulbrain Co. Ltd, Korea). Cyclic voltammetry (CV) and electrochemical impedance spectroscopy (EIS) studies were performed using a Bio-Logic (SP-150, France), electrochemical workstation. Galvanostatic charge-discharge studies were performed at conventional battery tester (WBCS 3000, Won-A-Tech, Korea) with ambient (25 °C) and elevated temperature (25 °C) conditions.

3. Results and discussion

The X-ray diffraction (XRD) patterns of the PJC's and PJAC were shown in Figure-1a and S1. The XRD patterns of PJC-1 and PJC-2 exhibits two broad reflections located at ~23 and 44°, which is associated with (002) and (110) planes of typical amorphous carbon, respectively. The intensity of (110) plane increases considerably with an increase in temperature from 900 to 1000 °C. Moreover, the KOH activation results (PJAC) the shifting of (002) plane peak position towards higher angle (~26°) with sharp reflections indicates that the formation of a high degree of crystalline strands *i.e.* graphitic carbons [27]. Moreover, the detailed structural information of PJC-2 and PJAC were studied by Raman spectroscopy and illustrated in Fig. 1b. These samples consisted of the characteristic D and G-bands and located at ~1345 and ~1577 cm^{-1}, respectively, which are corresponding to the defective and graphitic carbons [28–30]. A sharp 2D band (~2695 cm^{-1}) and the high I_G/I_D value (1.98) clearly indicates that PJAC was partially graphitized (*i.e.* few layered graphene) comparable to that of PJC-2 and well consistent with XRD measurements [31,32]. These results suggest that the added alkali ions (K^+) mainly remove the loosely bound

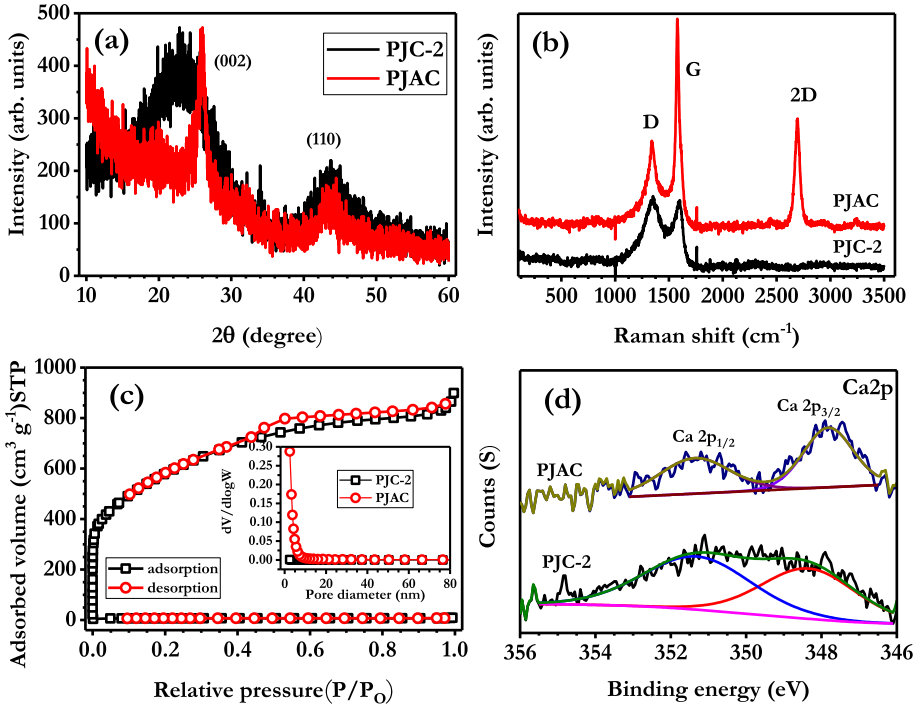

Fig. 1. The (a) XRD, (b) Raman spectra, (c) N_2 adsorption-desorption isotherm, and (d) XPS high resolution Ca 2p spectra of PJC-2 and PJAC.

carbon atoms from the (002) crystalline plane.

Figs. 1c and S2 shows the N_2-adsorption/desorption isotherms of PJCs. According to IUPAC classification, the PJAC isotherm belongs to Type-II with H4 hysteresis loop, which is a characteristic of micro- and macro-porous structure with interconnected pore geometry [33,34]. The inset in Fig. 1c clearly shows that the average pore size distribution is around 2.6 nm. The isotherm of the PJC-1 and PJC-2 increases at the high relative range ($0.9 < P/P_0$) implying the capillary condensation and multilayer sorption. The PJAC has an extremely high specific surface area compared with other samples. The calculated specific surface areas, total pore volume and pore diameter of the samples are given in the Table-1. Based on the specific surface area and Li-storage properties, we have chosen only the PJC-2 and PJAC materials for further studies.

The chemical composition and elemental chemical state of the PJC-2 and PJAC were studied with XPS as shown in Fig. 1d and Figure S2. The survey spectrum clearly revealed the presence of C, O, N, S and Ca elements. Fig. 1d The Ca 2p core-level spectrum assigned to the Ca^{2+} ions Ca $2p_{3/2}$ (~348.4 eV) and Ca $2p_{1/2}$ (~351.2 eV). Upon activation, the Ca 2p split into two main peaks with slight shifting towards lower energy level [35]. The spin-orbit splitting and full width at half maxima are estimated to 3.4 eV and 2.1 eV, which confirms that the Ca^{2+} ions most likely coordinated to the oxide and/or OH^- groups. As shown in Fig. S2, the high-resolution C 1s consisted of three peaks and it might be ascribed to the sp^2–C, O—C and O—C = O moieties of PJC-2 [36,37]. The O 1s de-convoluted spectrum clearly shows that the lower binding energy corresponds to the lattice bounded O^{2-} (O = C) and the higher energy peak originated from the oxygen-deficient chemisorbed species (O—C, O—C = O) [38]. The nitrogen (N 1s) and sulfur (S 2p) atoms are chemically bonded with carbon and it appears to be the pyrrolic-N (400.5 ± 0.3 eV) and C-SO_x (168.8 ± 0.3 eV), respectively [33,38,39].

Table 1
BET specific surface area, total pore volume and average pore diameter of the *Prosopis juliflora* derived carbons (PJC-1, PJC-2 & PJ-AC).

Samples	SBET[a] (m2 g−1)	Vtotal[b] (cm3 g−1)	Vmicro[c] (cm3 g−1)	Vmeso[d] (cm3 g−1)	Average pore diameter (nm)
PJC-1	25.4	0.0135	–	–	6.1
PJC-2	9.6	0.0162	–	–	2.1
PJ-AC	2082.8	1.3398	1.1261	0.2137	2.6

[a] S_{BET} is the BET surface area and it was measured at a relative pressure of 0.990.
[b] Total pore volume (V_{total}) was the single point adsorption total pore volume of pores less than 400 nm diameter at P/P_o = 0.990.
[c] V_{micro} is the micro-pore volume.

The scanning electron microscopic (SEM) images of the PJC-2 and PJAC are presented in Fig. 2. Fig. 2a and b shows the PJC-2 is naturally existing a hollow tube-like structure and the rigid carbon skeleton formed at high-temperature pyrolysis without any signs of cracking. As a consequence, the pre-treated char with KOH and the formed metallic potassium were effectively removed the low volatile and loosely bound cellulose contents. Thus creates the porous-structured carbon layers over the surface including inside the walls of the tubular structure is clearly evident from Fig. 2c and d.

The internal structure of the PJAC was examined in transmission electron microscopy (TEM) and given in Fig. 2e–h. As shown in Fig. 2e and f, it contains uneven sized both solid and transparent sheet-like carbons *i.e.* crystalline strands. These layered carbons are curled, twisted and randomly arranged in resulting highly disordered structure created by the low range structural rearrangements (or short range ordering). Moreover, the high-resolution TEM (HR-TEM) image of PJAC (Fig. 2g) represents the well-defined lattice fringes interlayer spacing of ~0.339 nm is consistent with d_{002} plane of graphitic carbon obtained by XRD (ICSD-980031170) measurements. In addition, the well-defined bright rings of selected area electron diffraction (SAED) pattern (see in Fig. 2h) indicates the crystalline nature of carbonaceous material synthesized. The measured *d*-spacing are 0.337, 0.203, 0.169 and 0.102 nm corresponding to the (002), (110), (004) and (331) crystallographic planes of the carbon.

The Li-storage performance of PJC-2 and PJAC materials were electrochemically evaluated in a half-cells *vs.* Li metal as shown in Fig. 3 and Figure S3. Fig. 3a and b displayed the galvanostatic charge-discharge profile of PJC-2, recorded at a current density of 0.1 A g^{-1} between 0 and 3 V. The initial lithiation and delithiation capacities of

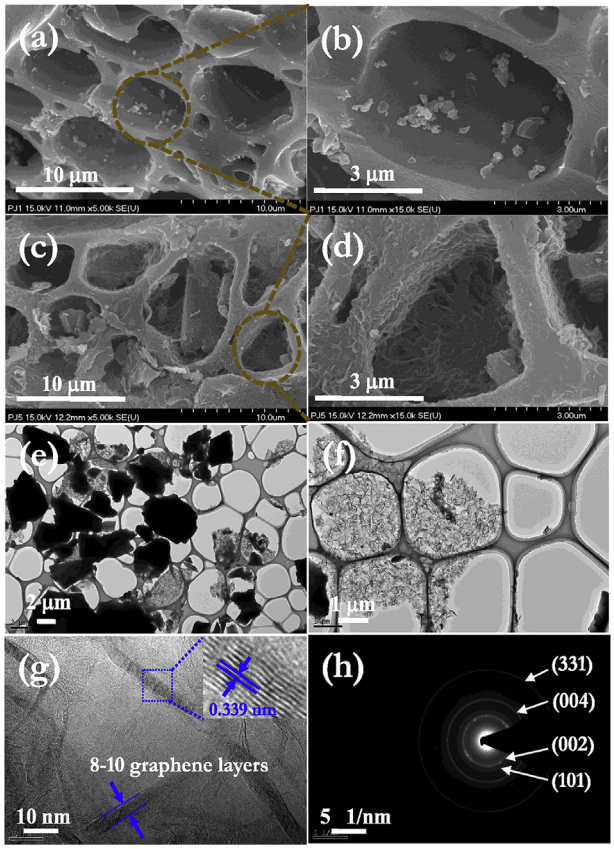

Fig. 2. SEM images of (a–b) PJC-2 and (c–d) PJAC. The (e–f) TEM, (g) HR-TEM and (h) SAED pattern of PJAC.

PJC-2 are found ~1408 and ~573 mAh g^{-1}, respectively. The charge-discharge curves are showing a sloping potential profile due to the amorphous nature of carbon [40]. The Li-intercalation process in PJC-2 is clearly understood from the differential capacity profile (Fig. S3). Briefly, after the 1st discharge, at below 1 V *vs.* Li, the broadened voltage profile is maintained up to 100 cycles indicating good reversible Li-insertion/extraction in/from the crystalline strands [11,12]. A very sharp and irreversible peak at ~0.8 V *vs.* Li is associated with the electrolyte decomposition upon first discharge. After the first cycle, the reversible capacity of ~490 mAh g^{-1} is maintained with ~99% of coloumbic efficiency for up to 100 cycles. Interestingly, the stabilized capacity is relatively higher than the theoretical capacity of long-range ordered graphite (372 mAh g^{-1}). More importantly, Fig. 3c showed an excellent rate capability performance at various current densities from 0.1 to 2 A g^{-1}, for example, the specific capacity of ~75 mAh g^{-1} is retained at a high current rate (2 A g^{-1}). Generally, the electrolyte reduction (< 1 V *vs.* Li) leads to the formation of solid electrolyte interphase (SEI) layer which eventually consumes Li in an irreversible manner. As a result, inferior coloumbic efficiency (~41%) is observed in the first cycle. The SEI layer is mandated for the safe operation of the insertion type carbonaceous anodes which effectively prevents the solvent molecule co-intercalation between the layers along with Li. Also, it protects the electrolyte solution as well, since the LiC_6 is very strong reductive agent [41]. Further, the presence of functional groups and defective sites offered bountiful binding and insertion sites, meanwhile can extract part of Li^+ smoothly from the deep inner sites of carbon. On the other hand in Fig. S4, the cathodic performance of PJAC was evaluated in the potential range of 2–4.6 V *vs.* Li at the current rate of 0.1 A g^{-1}. The cell delivered an initial discharge capacity of 149 mAh g^{-1} at the current rate of 0.1 A g^{-1} and showed a very stable cycle performance with an ~95% capacity retention over 100 cycles. The linear charge-discharge curves without plateaus indicate that the physical adsorption of ions over the surface of PJAC [42,43]. In other words, the PJAC involves a perfect double layer formation across the electrode-electrolyte interface. Interestingly, the observed capacity is much higher than the carbons in the similar configurations reported elsewhere [12,44–47] This impressive higher capacity and cycling stability results flare us to design the low cost and eco-friendly LIC from this prosopis juliflora derived carbons, specifically PJC-2 as (in pre-lithiated form) negative electrode and PJAC as the positive electrode.

Prior to LIC fabrication, the amorphous PJC-2 was pre-lithiated in a half cell *vs.* Li metal at 0.1 A g^{-1} current rate. After the three complete charge-discharge cycles, the cell was dismantled at the discharged state and coupled with the balanced loading of PJAC in LIC assembly. It is worth mention that, at discharged state, the mass of negative electrode (PJC-2) got increased ~16% ($2Li^+ + C_6 \leftrightarrow Li_2C_6$) [48,49]. Hence, the total mass of both electrode is calculated to be 11.6 g (1:4 ratio negative to the positive electrode) and it is based on the half-cell performance *vs.* Li. The LIC with pre-lithiated PJC-2//PJAC rendered an open circuit potential of ~3.1 V. Fig. 4 represents the CV curves and charge-discharge profile of LIC at different temperatures. Fig. 4a shows the CV traces of pre-lithiated PJC-2//PJAC based LIC at ambient temperature (25 °C) exhibits the quasi-rectangular shaped signatures without any specified/sharp redox peaks indicating that both electrodes are involving in the charge storage process. In a typical process, upon charge, the PF_6^- ions are migrated towards the positive electrode for double layer formation whereas Li^+ ions are intercalated to the crystalline strands of the negative electrode, and the said process is reversed during discharge. At higher scan rate, the curves are highly distorted indicating the perfect reversible non-Faradic capacitive reaction on the surface. Fig. 4b shows the galvanostatic charge-discharge curves of LIC displayed a non-linear slope with a plateau at above 3.2 V which corresponds to the (de-)intercalation of Li^+ ions. To further investigate, the electrochemical performance of LIC at 55 °C and presented in Fig. 4 c-d. The CV traces showed a well-defined (de-)intercalation peak at above 3.9 V, and the current response area underneath the CV curves is eventually reduced. Obviously, the charge-discharge plateau was consistent with the CV curve at 55 °C. This interesting high temperature behaviour of LIC clearly suggest that charge storage process is dominated by PJC-2 electrode than PJAC. Generally, at elevated temperature conditions, the electrolytes are prone to accelerate higher activity, specifically PF_6^- anions which vigorously involves decomposition process along with the solvent molecules. As a result, the SEI layer formed over PJC-2 the electrode gets thicker and thicker upon cycling, which eventually leads to the detrimental effect on the electrochemical activity. Also, the growth of the SEI layer certainly influence the cycling profile as well.

Fig. 4e shows the Nyquist plots of the pre-lithiated PJC-2//PJAC based LIC was measured at initial and after 5000 cycles at different temperatures. From the EIS traces, high to mid-frequency region arc is mainly consisted of the solution resistance (R_s) and charge transfer resistance (R_{ct}). The low-frequency region straight line slope suggesting faster Li^+ diffusion and better capacitive-like behaviour regardless of the temperatures [44]. The initial R_s and R_{ct} values of the LIC cell at 25 °C is calculated to be 5.10 and 12.26 Ω, respectively. After the cycling (5000 cycles), a significant decrement in internal resistances suggesting the increases of conductivity at the electrode/electrolyte interface (see in Table S1). However, at 55 °C, the R_{ct} of the LIC is increased to ~83 Ω which clearly parallels and supports the aforesaid statement for the formation of robust SEI layer.

The durability is another important feature of energy storage systems. The long-term cycling profile of the pre-lithiated PJC-2//PJAC based LIC at the current rate of 0.5 A g^{-1} was illustrated in Fig. 4f. The LIC exhibited superior cyclability with remarkable capacity retention characteristics of ~94% (~0.0013% capacity fading per cycle) after 5000 cycles at 25 °C. At high temperature (55 °C), as expected, slightly inferior retention properties are observed compared to room temperature performance, for example, only ~73% (0.0055% decay per cycle)

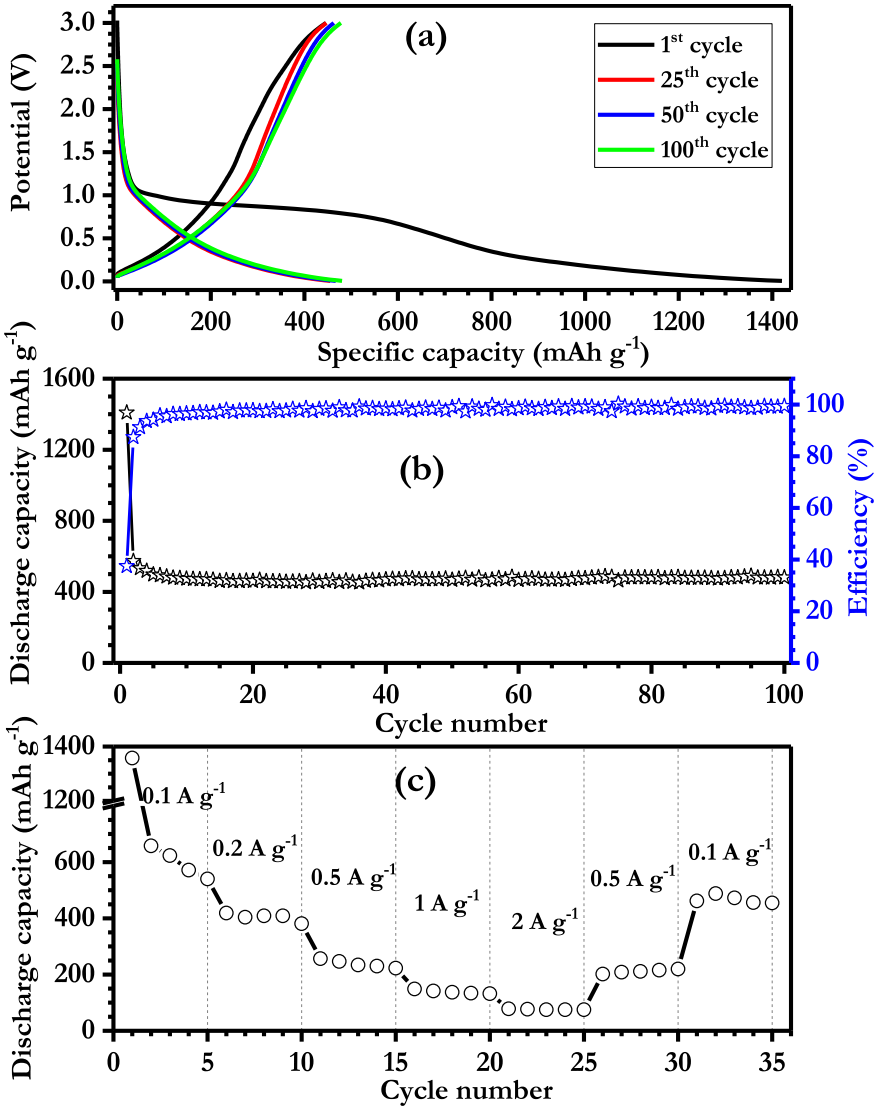

Fig. 3. (a) Galvanostatic charge-discharge profile and (b) cycling stability of PJC-2 as anode *vs.* Li at the current rate of 0.1 A g^{-1}, and (c) Rate capability studies of PJC-2 anode between 0 and 3 V *vs.* Li at 25 °C.

is retained. As mentioned, the inferior electrochemical activity at elevated temperature is associated with the unwanted side reaction with the electrolyte counterpart and subsequent growth of thick SEI layer. Apparently, in both temperature conditions, very high Coloumbic efficiency (> 99.8%) is maintained throughout the cycling.

Fig. 5 displays the Ragone plots of pre-lithiated PJC-2//PJAC based LIC supplemented with recently reported representative hybrid systems. The electrochemical parameters such as energy and power densities of the LIC were calculated from the following formulas, power density = [i (A) × ΔV]/[m (mg) × 10^{-6}] and energy density = [power density × Δt]/3600, where, "i" is the applied current (A), ΔV-average potential, m-total active material weight in both positive and negative electrode, Δt-total discharge time. Accordingly, the LIC delivered a very high energy density of ~216 Wh kg^{-1} with a power density of 155 W kg^{-1} at 25 °C, whereas ~186 Wh kg^{-1} only resulted at the elevated temperature (55 °C) conditions. Such performance is found superior compared with previously reported all carbon-based LIC systems, such as pre-lithiated graphite//AC [31], Amorphous carbon (AMC)//Porous disordered carbon sheet [50], pre-lithiated graphene//AC [51], flash reduced graphene oxide (FRGO)//3D graphene [52], N-rich carbon spheres (NRCS)//commercial AC [53]. The excellent electrochemical performance of pre-lithiated PJC-2//PJAC based LIC is mainly attributed to the tube-like structure along with the presence of hetero-atoms like N, S, and Ca, active surface functional groups and defects. More importantly, the utilization of amorphous carbon along with crystalline strands cannot be ruled out which not only provides the facile Li-intercalation process and conductivity, also translates better compatibility with KOH treated counter electrode and enables the better Li-storage capability to yield high energy density.

We successfully synthesized, and efficiently utilized the amorphous tube-like carbon with crystalline strands from the invasive prosopis juliflora bio-source through a carbonization process. Presence of amorphous and crystalline strands synergistically offer additional Li^+ storage sites on the surface and the interlayers. The activated carbon was obtained by KOH treatment exhibited high surface area with hierarchical porosity. Both activated carbon and amorphous carbon with crystalline strands rendered high capacity and good cycling profiles in half-cell configuration. Owing to the beneficial features, the PJC-2//PJAC based LIC was fabricated and delivered a maximum energy density of ~216 Wh kg^{-1} at ambient temperature with excellent cycling profiles. In contrary, at high-temperature operation, slightly inferior performance is noted because of the accelerated activity with the electrolyte solution and its decomposition. Overall, our work emphasized that the invasive prosopis juliflora bio-source can be

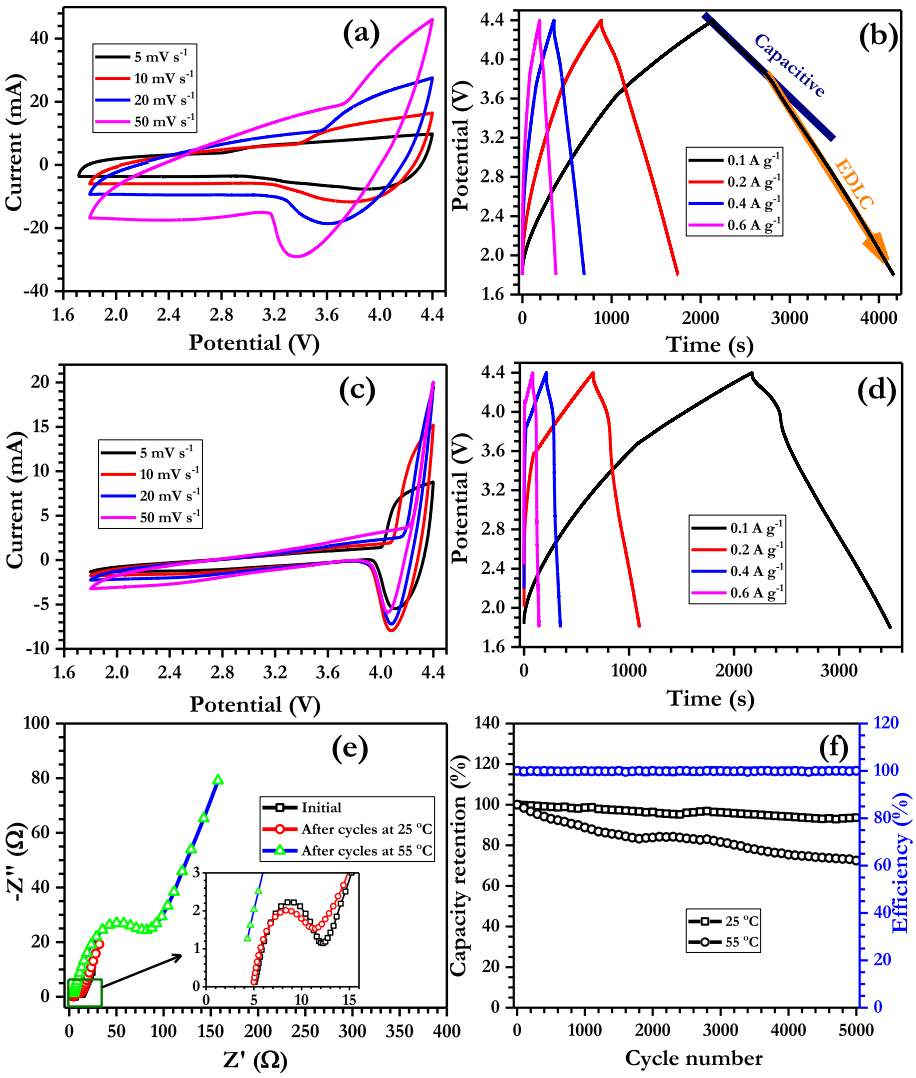

Fig. 4. The cyclic voltammograms and charge-discharge profile of the pre-lithiated PJC-2//PJ-AC based LIC at different temperatures (a–b) 25 °C and (c–d) 55 °C, (e) Nyquist plots before and after cycling, and (f) cycling profile of LIC cell at current density of 0.5 A g^{-1} in 25 and 55 °C.

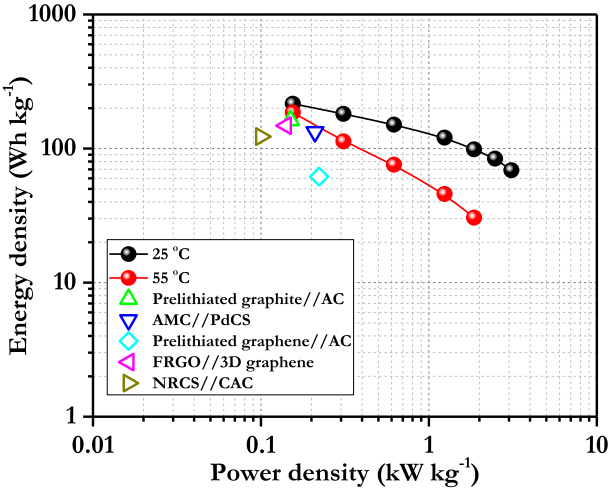

Fig. 5. Ragone plots of the pre-lithiated PJC-2//PJAC based LIC at 25 and 55 °C.

efficiently utilized as low-cost high-performance materials to build next-generation hybrid energy storage systems and capable of delivering remarkable performance at different temperatures. This not only provides the high-performance active material for charge storage systems *via* "waste-to-wealth" approach, also beneficial for the betterment of environmental aspects.

Acknowledgment

This study was supported by the National Research Foundation of Korea grant funded by the Korea government (Ministry of Science, ICT) (No. NRF-2011-C1AAA0010030538). Also, the work was financially supported by NTU-HUJ Create Phase II which is a joint research programme between the Hebrew University of Jerusalem (HUJ, Israel) and Nanyang Technological University (NTU, Singapore) with CREATE (Campus for Research Excellence and Technological Enterprise) funding from National Research Foundation of Singapore (NRF,Singapore). VA thank the financial support from the Science & Engineering Research Board (SERB), a statutory body of the Department of Science & Technology, Govt. of India through Ramanujan Fellowship (SB/S2/RJN-088/2016).

Appendix A. Supplementary data

Supplementary data to this article can be found online at https://doi.org/10.1016/j.jpowsour.2018.12.089.

References

[1] P. Simon, P.-L. Taberna, F. Béguin, Electrical Double-Layer Capacitors and Carbons for EDLCs, Supercapacitors, Wiley-VCH Verlag GmbH & Co. KGaA, Weinheim, Germany, 2013, pp. 131–165.
[2] A.D. Pasquier, I. Plitz, J. Gural, F. Badway, G.G. Amatucci, Power-ion battery: bridging the gap between Li-ion and supercapacitor chemistries, J. Power Sources 136 (1) (2004) 160–170.
[3] G.G. Amatucci, F. Badway, A. Du Pasquier, T. Zheng, An asymmetric hybrid nonaqueous energy storage cell, J. Electrochem. Soc. 148 (8) (2001) A930–A939.
[4] B. Akinwolemiwa, C. Peng, G.Z. Chen, Redox electrolytes in supercapacitors, J. Electrochem. Soc. 162 (5) (2015) A5054–A5059.
[5] V. Aravindan, J. Gnanaraj, Y.-S. Lee, S. Madhavi, Insertion-type electrodes for nonaqueous Li-ion capacitors, Chem. Rev. 114 (23) (2014) 11619–11635.
[6] V. Aravindan, Y.-S. Lee, Building next-generation Li-ion capacitors with high energy: an approach beyond intercalation, J. Phys. Chem. Lett. (2018) 3946–3958.
[7] P. Simon, Y. Gogotsi, B. Dunn, Where do batteries end and supercapacitors begin? Science 343 (6176) (2014) 1210–1211.
[8] A. Balducci, D. Belanger, T. Brousse, J.W. Long, W. Sugimoto, Perspective—a guideline for reporting performance metrics with electrochemical capacitors: from electrode materials to full devices, J. Electrochem. Soc. 164 (7) (2017) A1487–A1488.
[9] R. Yazami, P. Touzain, A reversible graphite-lithium negative electrode for electrochemical generators, J. Power Sources 9 (3) (1983) 365–371.
[10] R. Yazami, P. Touzain, Lithium — graphite oxide cells Part III: effect of origin and oxidation of graphite on batteries performances, Synth. Met. 12 (1–2) (1985) 499–503.
[11] T. Sri Devi Kumari, A.J.J. Jebaraj, T.A. Raj, D. Jeyakumar, T.P. Kumar, A kish graphitic lithium-insertion anode material obtained from non-biodegradable plastic waste, Energy 95 (Supplement C) (2016) 483–493.
[12] S. Jayaraman, G. Singh, S. Madhavi, V. Aravindan, Elongated graphitic hollow nanofibers from vegetable oil as prospective insertion host for constructing advanced high energy Li-Ion capacitor and battery, Carbon 134 (2018) 9–14.
[13] H. Lu, X.S. Zhao, Biomass-derived carbon electrode materials for supercapacitors, Sustainable Energy & Fuels 1 (6) (2017) 1265–1281.
[14] Y. Yao, F. Wu, Naturally derived nanostructured materials from biomass for rechargeable lithium/sodium batteries, Nanomater. Energy 17 (2015) 91–103.
[15] J. Niu, R. Shao, J. Liang, M. Dou, Z. Li, Y. Huang, F. Wang, Biomass-derived mesopore-dominant porous carbons with large specific surface area and high defect density as high performance electrode materials for Li-ion batteries and supercapacitors, Nanomater. Energy 36 (2017) 322–330.
[16] J. Niu, R. Shao, M. Liu, J. Liang, Z. Zhang, M. Dou, Y. Huang, F. Wang, Porous carbon electrodes with battery-capacitive storage features for high performance Li-ion capacitors, Energy Storage Materials 12 (2018) 145–152.
[17] P. Simon, Y. Gogotsi, Materials for electrochemical capacitors, Nat. Mater. 7 (11) (2008) 845–854.
[18] W. Yu, H. Wang, S. Liu, N. Mao, X. Liu, J. Shi, W. Liu, S. Chen, X. Wang, N, O-codoped hierarchical porous carbons derived from algae for high-capacity supercapacitors and battery anodes, J. Mater. Chem. 4 (16) (2016) 5973–5983.
[19] T. Brousse, D. Bélanger, J.W. Long, To Be or not to Be pseudocapacitive? J. Electrochem. Soc. 162 (5) (2015) A5185–A5189.
[20] J. Wang, P. Nie, B. Ding, S. Dong, X. Hao, H. Dou, X. Zhang, Biomass derived carbon for energy storage devices, J. Mater. Chem. 5 (6) (2017) 2411–2428.
[21] M. Biswal, A. Banerjee, M. Deo, S. Ogale, From dead leaves to high energy density supercapacitors, Energy Environ. Sci. 6 (4) (2013) 1249–1259.
[22] T. Brousse, D. Bélanger, D. Guay, Asymmetric and Hybrid Devices in Aqueous Electrolytes, Supercapacitors, Wiley-VCH Verlag GmbH & Co. KGaA, Weinheim, Germany, 2013, pp. 257–288.
[23] E. Frackowiak, Electrode Materials with Pseudocapacitive Properties, Supercapacitors, Wiley-VCH Verlag GmbH & Co. KGaA, Weinheim, Germany, 2013, pp. 207–237.
[24] G.A.d.B. Damasceno, M. Ferrari, R.B. Giordani, Prosopis juliflora (SW) D.C., an invasive specie at the Brazilian Caatinga: phytochemical, pharmacological, toxicological and technological overview, Phytochemistry Rev. 16 (2) (2017) 309–331.
[25] R.T. Shackleton, D.C. Le Maitre, N.M. Pasiecznik, D.M. Richardson, Prosopis: a global assessment of the biogeography, benefits, impacts and management of one of the world's worst woody invasive plant taxa, AoB PLANTS 6 (2014) plu027-plu027.
[26] S. Ruiying, H. Cuiping, X. Xiaofu, Q. Xianying, X. Lei, L. Hongfei, L. Junqin, W. Ching-Ping, L. Baohua, Electrospun N-doped hierarchical porous carbon nanofiber with improved degree of graphitization for high-performance lithium ion capacitor, Chem. Eur J. 24 (41) (2018) 10460–10467.
[27] Z.Q. Li, C.J. Lu, Z.P. Xia, Y. Zhou, Z. Luo, X-ray diffraction patterns of graphite and turbostratic carbon, Carbon 45 (8) (2007) 1686–1695.
[28] A.C. Ferrari, D.M. Basko, Raman spectroscopy as a versatile tool for studying the properties of graphene, Nat. Nanotechnol. 8 (4) (2013) 235–246.
[29] A.C. Ferrari, J. Robertson, Interpretation of Raman spectra of disordered and amorphous carbon, Phys. Rev. B 61 (20) (2000) 14095–14107.
[30] F. Tuinstra, J.L. Koenig, Raman spectrum of graphite, J. Chem. Phys. 53 (3) (1970) 1126–1130.
[31] S. Palanichamy, A. Vanchiappan, G. Mahadevan, L. Young-Gi, L. Yun-Sung, Biomass-derived electrode for next generation lithium-ion capacitors, ChemSusChem 9 (8) (2016) 849–854.
[32] K.S. Rao, J. Senthilnathan, Y.-F. Liu, M. Yoshimura, Role of peroxide ions in formation of graphene nanosheets by electrochemical exfoliation of graphite, Sci. Rep. 4 (2014) 4237.
[33] D. Nan, Z.-H. Huang, R. Lv, L. Yang, J.-G. Wang, W. Shen, Y. Lin, X. Yu, L. Ye, H. Sun, F. Kang, Nitrogen-enriched electrospun porous carbon nanofiber networks as high-performance free-standing electrode materials, J. Mater. Chem. 2 (46) (2014) 19678–19684.
[34] J. Wang, S. Kaskel, KOH activation of carbon-based materials for energy storage, J. Mater. Chem. 22 (45) (2012) 23710–23725.
[35] J. Baltrusaitis, C.R. Usher, V.H. Grassian, Reactions of sulfur dioxide on calcium carbonate single crystal and particle surfaces at the adsorbed water carbonate interface, Phys. Chem. Chem. Phys. 9 (23) (2007) 3011–3024.
[36] Q. Wang, L. Jiao, H. Du, Y. Si, Y. Wang, H. Yuan, Co3S4 hollow nanospheres grown on graphene as advanced electrode materials for supercapacitors, J. Mater. Chem. 22 (40) (2012) 21387–21391.
[37] G. Wang, J. Zhang, S. Kuang, S. Liu, S. Zhuo, The production of cobalt sulfide/graphene composite for use as a low-cost counter-electrode material in dye-sensitized solar cells, J. Power Sources 269 (2014) 473–478.
[38] Z. Yang, M. Xu, Y. Liu, F. He, F. Gao, Y. Su, H. Wei, Y. Zhang, Nitrogen-doped, carbon-rich, highly photoluminescent carbon dots from ammonium citrate, Nanoscale 6 (3) (2014) 1890–1895.
[39] B. Kumar, M. Asadi, D. Pisasale, S. Sinha-Ray, B.A. Rosen, R. Haasch, J. Abiade, A.L. Yarin, A. Salehi-Khojin, Renewable and metal-free carbon nanofibre catalysts for carbon dioxide reduction, Nat. Commun. 4 (2013) 2819.
[40] T. Prem Kumar, T. Sri Devi Kumari, A. Manuel Stephan, Carbonaceous anode materials for lithium-ion batteries-the road ahead, J. Indian Inst. Sci. 89 (4) (2009) 393–424.
[41] E. Peled, S. Menkin, Review—sei: past, present and future, J. Electrochem. Soc. 164 (7) (2017) A1703–A1719.
[42] S. Jayaraman, A. Jain, M. Ulaganathan, E. Edison, M.P. Srinivasan, R. Balasubramanian, V. Aravindan, S. Madhavi, Li-ion vs. Na-ion capacitors: a performance evaluation with coconut shell derived mesoporous carbon and natural plant based hard carbon, Chem. Eng. J. 316 (2017) 506–513.
[43] T. Aida, K. Yamada, M. Morita, An advanced hybrid electrochemical capacitor that uses a wide potential range at the positive electrode, Electrochem. Solid State Lett. 9 (12) (2006) A534–A536.
[44] F. Sun, X. Liu, H.B. Wu, L. Wang, J. Gao, H. Li, Y. Lu, In situ high-level nitrogen doping into carbon nanospheres and boosting of capacitive charge storage in both anode and cathode for a high-energy 4.5 V full-carbon lithium-ion capacitor, Nano Lett. 18 (6) (2018) 3368–3376.
[45] S. Jayaraman, S. Madhavi, V. Aravindan, High energy Li-ion capacitor and battery using graphitic carbon spheres as an insertion host from cooking oil, J. Mater. Chem. 6 (7) (2018) 3242–3248.
[46] X. Qiuying, Y. Hai, W. Min, Y. Mei, G. Qiubo, W. Liming, X. Hui, Y. Yan, High energy and high power lithium-ion capacitors based on boron and nitrogen dual-doped 3D carbon nanofibers as both cathode and anode, Advanced Energy Materials 7 (22) (2017) 1701336.
[47] L. Shaohui, C. Jingwei, C. Mengqi, C. Guofa, W. Jiangxin, C. Peng, G. Xuefei, L. P, See, a high-performance lithium-ion capacitor based on 2D nanosheet materials, Small 13 (6) (2017) 1602893.
[48] Y. Liu, J.S. Xue, T. Zheng, J.R. Dahn, Mechanism of lithium insertion in hard carbons prepared by pyrolysis of epoxy resins, Carbon 34 (2) (1996) 193–200.
[49] J.R. Dahn, T. Zheng, Y. Liu, J.S. Xue, Mechanisms for lithium insertion in carbonaceous materials, Science 270 (5236) (1995) 590–593.
[50] W.S.V. Lee, X. Huang, T.L. Tan, J.M. Xue, Low Li + insertion barrier carbon for high energy efficient lithium-ion capacitor, ACS Appl. Mater. Interfaces 10 (2) (2018) 1690–1700.
[51] J.J. Ren, L.W. Su, X. Qin, M. Yang, J.P. Wei, Z. Zhou, P.W. Shen, Pre-lithiated graphene nanosheets as negative electrode materials for Li-ion capacitors with high power and energy density, J. Power Sources 264 (2014) 108–113.
[52] T. Zhang, F. Zhang, L. Zhang, Y. Lu, Y. Zhang, X. Yang, Y. Ma, Y. Huang, High energy density Li-ion capacitor assembled with all graphene-based electrodes, Carbon 92 (2015) 106–118.
[53] F. Sun, J. Gao, X. Liu, L. Wang, Y. Yang, X. Pi, S. Wu, Y. Qin, High-energy Li-ion hybrid supercapacitor enabled by a long life N-rich carbon based anode, Electrochim. Acta 213 (2016) 626–632.